

# Stereodirection of an $\alpha$ -Ketoester at Sub-molecular Sites on Chirally Modified Pt(111): Heterogeneous Asymmetric Catalysis

Vincent Demers-Carpentier,<sup>†</sup> Anton M. H. Rasmussen,<sup>‡</sup> Guillaume Goubert,<sup>†</sup> Lara Ferrighi,<sup>‡</sup> Yi Dong,<sup>†</sup> Jean-Christian Lemay,<sup>†</sup> Federico Masini,<sup>†</sup> Yang Zeng,<sup>†</sup> Bjørk Hammer,<sup>\*,‡</sup> and Peter H. McBreen<sup>\*,†</sup>

<sup>†</sup>C3V and Department of Chemistry, Laval University, Québec, Canada G1V 0A6

<sup>‡</sup>Interdisciplinary Nanoscience Center (iNano) and Department of Physics and Astronomy, Aarhus University, DK 8000 Aarhus, Denmark

**S** Supporting Information

**ABSTRACT:** Chirally modified Pt catalysts are used in the heterogeneous asymmetric hydrogenation of  $\alpha$ -ketoesters. Stereinduction is believed to occur through the formation of chemisorbed modifier–substrate complexes. In this study, the formation of diastereomeric complexes by coadsorbed methyl 3,3,3-trifluoropyruvate, MTFP, and (*R*)-(+)-1-(1-naphthyl)ethylamine, (*R*)-NEA, on Pt(111) was studied using scanning tunneling microscopy and density functional theory methods. Individual complexes were imaged with sub-molecular resolution at 260 K and at room temperature. The calculations find that the most stable complex isolated in room-temperature experiments is formed by the minority rotamer of (*R*)-NEA and pro-*S* MTFP. The stereodirecting forces in this complex are identified as a combination of site-specific chemisorption of MTFP and multiple non-covalent attractive interactions between the carbonyl groups of MTFP and the amine and aromatic groups of (*R*)-NEA.

The formation of short-lived non-covalently bonded complexes on surfaces is fundamental to many chiral discrimination methods<sup>1</sup> and to the enantioselective hydrogenation of  $\alpha$ -ketoesters at sites created by chiral molecules on platinum catalysts.<sup>2,3</sup> The latter family of reactions is believed to involve 1:1 complexation between the chiral modifier and the prochiral substrate, on the metal surface, prior to hydrogenation.<sup>3,4</sup> The interdependence of the chemisorption and intermolecular interactions operating in such diastereomeric complexes has yet to be comprehensively investigated. Only recently has the direct observation of such complexes become possible.<sup>5</sup>

In this study, we use a combination of scanning tunneling microscopy (STM) and density functional theory (DFT) methods to probe complexes formed by methyl 3,3,3-trifluoropyruvate, MTFP, and (*R*)-(+)-1-(1-naphthyl)ethylamine, (*R*)-NEA, on Pt(111). The (*R*)-NEA/MTFP chiral–prochiral pair was chosen to mimic the heterogeneous enantioselective hydrogenation of methyl pyruvate on Pt/Al<sub>2</sub>O<sub>3</sub> modified by an NEA condensate.<sup>6</sup> MTFP, rather than methyl pyruvate, was used so as to avoid keto–enol tautomerization and consequent self-assembly into chains on the metal surface.<sup>7</sup> In previous work, we have studied complexes formed between

(*R*)-NEA and an  $\alpha$ -phenyl ketone substrate.<sup>5</sup> The latter study revealed a hierarchy of chemisorption and intermolecular interactions, including both N–H $\cdots$ O bonding<sup>4c,d</sup> and steric repulsion, leading to specific prochiral ratios at individual sites around the ethylamine group of (*R*)-NEA.

The scanning tunneling microscopy experiments were performed under the room-temperature conditions typically used in the enantioselective hydrogenation of  $\alpha$ -ketoesters on Pt.<sup>2,3</sup> Measurements were also performed at 260 K. In modeling the platinum surface we employed a c(12 $\times$ 6) slab of four layers, each with 36 metal atoms. The electronic interactions were approximated using the meta-GGA M06-L exchange-correlation density functional.<sup>8</sup> This functional is constructed to describe dispersion interactions and is able to properly describe the hydrogen bonds present in the molecular complexes of our study. In our analysis, we assume that both MTFP and (*R*)-NEA are adsorbed intact in the STM experiments. This assumption is supported by reflectance absorbance infrared spectroscopy (RAIRS) measurements (see the Supporting Information (SI)).

As reported previously, (*R*)-NEA forms two rotamers on Pt(111) in a ratio of approximately 70:30 at room temperature.<sup>5</sup> We label the majority rotamer (*R*)-NEA-1 and the minority rotamer (*R*)-NEA-2. As determined by DFT calculations (see Figures 2 and 3), the most stable (*R*)-NEA-2 adsorption geometry is an *endo*-conformation where the amine points toward the non-substituted ring.<sup>5</sup> In the present meta-GGA-based DFT investigation, the calculated adsorption geometries are essentially unaltered with respect to the previously reported structures,<sup>5</sup> and the calculated adsorption energies of the (*R*)-NEA-1 and (*R*)-NEA-2 rotamers are  $-2.24$  and  $-2.06$  eV, respectively. The bright protrusion in the STM images of (*R*)-NEA is assigned to the ethylamine group and the dimmer oval-shaped protrusion to the naphthyl group, by reference to simulated images and to data for related molecules.<sup>5</sup> The (*R*)-NEA-2 rotamer may be visually distinguished (Figure 1A,B) by noting that the bright feature is located to the far left.<sup>5</sup> Analogous observations were reported by Tysoe et al. for NEA on Pd(111).<sup>9</sup>

Isolated 1:1 and termolecular complexes were formed on coadsorption of (*R*)-NEA and MTFP (Figure 1). MTFP was

Received: April 21, 2013

Published: June 20, 2013

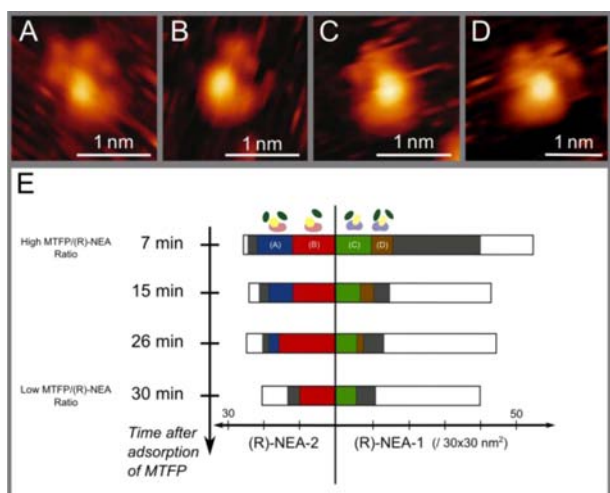


**Figure 1.** STM images of (*R*)-NEA and MTFP on Pt(111) at room temperature: (A) (MTFP)<sub>2</sub>/*(R)*-NEA-2 complex, (B) 1:1 MTFP/*(R)*-NEA-2 complex, (C) 1:1 MTFP/*(R)*-NEA-1 complex, and (D) (MTFP)<sub>2</sub>/*(R)*-NEA-1 complex. (E) Change as a function of time in the number of complexes observed in a 30 × 30 nm<sup>2</sup> area during a room-temperature experiment. The blue, green, red, and brown segments represent families of complexes in which MTFP is found to the left or right of the bright protrusion. The gray segment represents all other complexes, including very poorly resolved ones. The non-colored segments indicate the number of noncomplexed (*R*)-NEA rotamers. The variation in the total number of (*R*)-NEA is due to changes in the specific area imaged. The imaging conditions were 1.0 V sample bias and 0.25 nA tunnel current.

only imaged in complexes, reflecting its immobilization by the modifier. The majority of complexed MTFP is found either to the right or the left-hand side of the ethylamine group under conditions where roughly half of the total number of imaged (*R*)-NEA molecules occur in complexes. Time-lapsed images taken at room temperature revealed a dynamic system where the complexes displayed apparent lifetimes ranging from less than 30 s to a few minutes. Supporting RAIRS data show that MTFP begins to desorb from clean Pt(111) at approximately 260 K. As a result of MTFP desorption, the number of complexes decreases continuously during the course of a given room-temperature experiment (Figure 1E). This change is also seen as a decrease in the ratio of termolecular, (MTFP)<sub>2</sub>/*(R)*-NEA, to 1:1 complexes. The most abundant and long-lived complexes observed under such dynamic conditions are also the most stable complexes. Figure 1B shows the most abundant complex at low relative coverages of MTFP.

In the most stable (*R*)-NEA-2 complex, MTFP is located on the right-hand side in the cradle formed by the ethylamine group and the non-substituted aromatic ring. STM imaging at 260 K shows that in this complex MTFP appears as two touching round protrusions, of unequal size (Figure 3A). The same sub-molecular motif is sometimes also resolved in the room-temperature measurements (Figure 1B), reflecting the relatively long lifetime and rigidity of the most stable complex. A distinction can be made between the bigger and smaller protrusion in roughly 75% of the images of this complex at 260 K (Figure 3A), and in a smaller fraction of the corresponding room-temperature images (Figure 1B). Significantly, in all cases, the biggest protrusion is located close to the top right-hand side of the ethylamine-derived bright protrusion while the smaller one is located closer to the non-substituted aromatic

ring. This persistent configuration shows a clearly preferred directionality of MTFP relative to (*R*)-NEA-2 in the most stable 1:1 complex.

A DFT investigation was carried out to examine the forces driving complexation. The chemisorption of MTFP on the bare Pt(111) surface was studied first. In the distinctly most stable structure found (Figures 2A and SI) the potential energy gain is

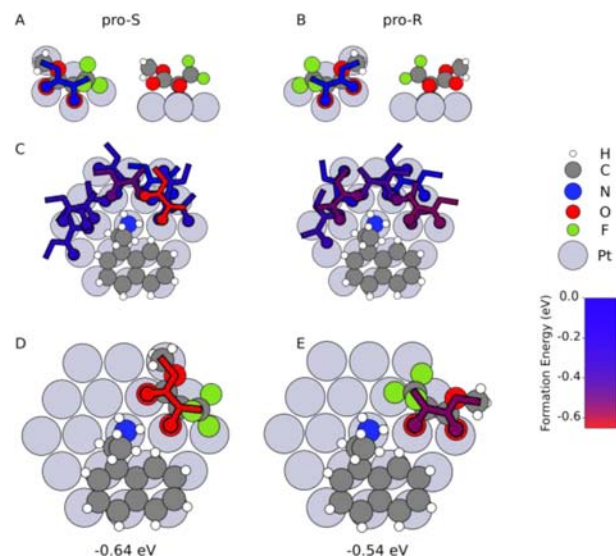


**Figure 2.** (A,B) Pro-S and pro-R MTFP configurations of the most stable calculated adsorption structure of MTFP on Pt(111). (C) Systematic DFT search for the most stable complexes formed between MTFP and (*R*)-NEA-2. The color code indicates the formation energy of each specific complex. (D,E) The two most stable complexes found in the search.

0.75 eV. MTFP is in the *cis*-conformation with the keto-CO bond bridged between two Pt atoms in an  $\eta^2$ -configuration. The strongly perturbed carbonyl bond is elongated to 1.34 Å from the calculated gas-phase value of 1.20 Å, and is aligned approximately 6° off the direction of the close-packed Pt rows. This faint rotation places the oxygen atom of the ester-CO hovering over a Pt-atom, with the ester-CO bond tilted toward the Pt-atom and elongated only slightly (SI). The distance between the ester carbonyl oxygen and the underlying Pt atom is 2.24 Å. The energetically equivalent mirror form of the MTFP adsorption state is illustrated in Figure 2B. The surface enantiomers, 2A and B, are labeled as pro-S and pro-R MTFP, respectively, in terms of the absolute configuration of the hydroxy ester product that would be formed by hydrogenation at the enantioface turned toward the metal surface.

Next, a systematic DFT search for the most stable 1:1 (*R*)-NEA-2 complex was conducted. The site-specific chemisorption of MTFP limits the number of possible geometries. The investigated ones are illustrated in Figure 2C. The most stable of all the complexes studied is shown in Figure 2D. In this structure, pro-S MTFP is located to the right of the ethylamine group and the keto-carbonyl oxygen is placed atop the platinum atom in the chiral space in proximity to the NH<sub>2</sub> group and the  $\alpha$ -CH of the non-substituted aromatic ring. This permits the keto-carbonyl to undergo simultaneous aryl-CH $\cdots$ OC<sub>keto</sub> and NH $\cdots$ OC<sub>keto</sub> interactions, while maintaining an  $\eta^2$ -chemisorption interaction. It also permits the ester carbonyl to form an NH $\cdots$ OC<sub>ester</sub> bond to the amine group.

The calculations thus reveal that the distinctly most stable (*R*)-NEA-2 complex involves two-point/two-carbonyl intermolecular bonding. The resulting formation energy added to the surface diffusion energy traps MTFP into relatively long-lived complexes. Multiple bonding in these complexes causes conformational rigidity that in turn allows sub-molecular resolution even under the highly dynamic conditions of the room-temperature experiments (Figure 1B). The dynamic nature of a room-temperature experiment, in which complexes form and break regularly at the time scale of the experiment, facilitates the isolation of the most stable complexes. The DFT simulated image of the most stable (*R*)-NEA-2 complex provides an excellent match to the STM image of the experimentally isolated complex, both at room temperature (Figure 1B) and at 260 K (Figure 3A). The simulated image

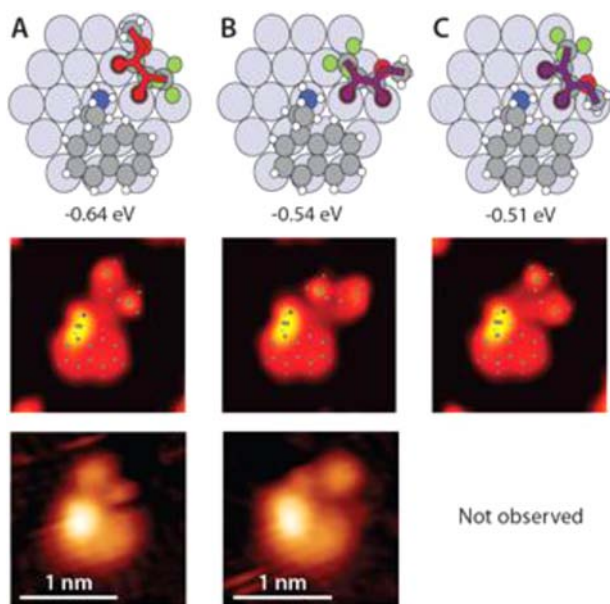


**Figure 3.** (Top) The two most stable (*R*)-NEA-2/MTFP complexes found by DFT calculations. (Middle) Corresponding simulated images. (Bottom) Corresponding STM images observed at 260 K.

clearly shows the double protrusion motif, with the larger protrusion arising from the ester moiety. The simulated image also faithfully reproduces the directionality of the measured STM image with the smaller protrusion pointing toward the non-substituted aromatic ring. We note that the same small protrusion/big protrusion motif is also clearly resolved in ((*R*)-NEA)<sub>2</sub>/MTFP complexes (SI), a case where we assume that each of the two carbonyls is bonded to a separate modifier molecule.

Images consistent with two-point bonding into the pro-R structure shown in Figure 3C were never observed in our STM experiments. That is, a mirror image motif of the most abundant (*R*)-NEA-2 complex, where the smaller protrusion points toward the ethylamine group and the larger one to the non-substituted aromatic ring, was never observed. In order to understand the relative instability of such a pro-R complex, it is critical to understand why the ester-carbonyl does not successfully compete with the keto-carbonyl to form a combined aryl-CH $\cdots$ OC<sub>ester</sub> and NH<sub>2</sub> $\cdots$ OC<sub>ester</sub> interaction. In answer to this question, DFT calculations (Figure 3C, and SI) find that interchanging the keto-CO and ester-CO positions by flipping MTFP to give a two-point bonding pro-R config-

uration, results in a complex that is 0.13 eV less strongly bound. In this configuration, the ester carbonyl oxygen relaxes into a position 3.23 Å above the Pt-atom, in contrast to 2.24 Å for the most stable isolated MTFP structure and 2.90 Å for the most stable complex. Thus, it appears that the ester carbonyl oxygen in the two-point bonded pro-R complex cannot simultaneously interact optimally with both the metal surface and the modifier. In contrast, (*R*)-NEA-2 preferentially binds MTFP in the pro-S configuration (Figures 2D and 3A), where the combination of intermolecular and chemisorption interactions can be best satisfied. The clearly preferred set of interactions identified by the calculations explains the unique directionality in the sub-molecularly resolved STM images of the most stable complex (Figures 1B and 3A).

The second most stable 1:1 (*R*)-NEA-2 complex predicted by DFT (Figure 2E) was isolated (Figure 3B) in very low abundances (less than 5% of the population of the most stable complex) in STM experiments performed at 260 K. The experimental and simulated data for this pro-R complex are in close agreement, in that in both cases the smaller protrusion points toward the ethylamine group but the large protrusion does not point toward the aromatic ring. This directionality is consistent with the calculated structure showing intermolecular bonding through the keto-carbonyl alone, forming simultaneous aryl-CH $\cdots$ OC<sub>keto</sub> and NH $\cdots$ OC<sub>keto</sub> interactions. The calculated energy difference of 0.1 eV between the two most stable complexes is consistent with their relative abundances. The study thus shows that the chiral pocket described by the cradle formed by the ethylamine and non-substituted aromatic ring displays very strong stereochemical bias toward pro-S complexation. Calculations involving methyl pyruvate (SI), where CF<sub>3</sub> is substituted by CH<sub>3</sub>, show pro-R selectivity as a result of the same stereodirecting interactions as found for MTFP. The change in prochirality simply results from the application of the Cahn–Ingold–Prelog priority rule on replacing CF<sub>3</sub> by CH<sub>3</sub>. These findings are consistent with the stereoselectivity observed for  $\alpha$ -ketoesters on Pt catalysts modified using (*R*)-NEA and (*R*)-NEA derivatives.<sup>6</sup>

In summary, this study reveals that combined chemisorption and multiple non-covalent bonding interactions at (*R*)-NEA-2 preferentially impose a pro-S configuration on MTFP in the most stable complex formed at room temperature. With respect to the DFT determined  $\eta^2$ -(Pt-O-C-Pt) adsorption of the keto-carbonyl, we note that a *di*-sigma configuration has been proposed as the active species in the asymmetric hydrogenation of  $\alpha$ -ketoesters on chirally modified Pt.<sup>10</sup> Furthermore, multiple non-covalent interactions are central to effective organocatalysis.<sup>11</sup> Hence we expect the ones operating in the modifier–substrate complexes to contribute, in addition to chemisorption, to the activation of the keto-carbonyl. Such combined activation may play a role in the rate enhancement of the enantioselective reaction that is often a feature of the hydrogenation of methyl pyruvate and other  $\alpha$ -ketoesters on chirally modified platinum.<sup>3</sup>

The structure of the most stable (*R*)-NEA-2 complex is in general agreement with a simple model that we proposed for the stereodirecting action of NEA on  $\alpha$ -ketoesters on Pt.<sup>4f,12</sup> However, the present study reveals several levels of complexity. The STM measurements performed at 260 K confirm that (*R*)-NEA-1 and (*R*)-NEA-2, in combination, present several chiral pockets to MTFP on Pt(111). MTFP forms complexes at the right, left, and top of the ethylamine group of both conformers. Both pro-R and pro-S complexes are formed. At relatively low

MTFP to (R)-NEA coverages, the minority conformer, (R)-NEA-2, forms proportionately more complexes (Figure 1E). Different complexes display different lifetimes. The overall enantioselective induction in such a system would depend on the populations and prochiral ratios specific to each chiral pocket, and on relative rates of hydrogenation. While we can discuss the population of different complexes we cannot safely predict the enantioselectivity of the hydrogenation reaction since our energy calculations only concern energy minima, not reaction paths. Stereochemical kinetics and dynamics will be addressed in future studies.

## ■ ASSOCIATED CONTENT

### ■ Supporting Information

Experimental methods and STM, DFT, and RAIRS data. This material is available free of charge via the Internet at <http://pubs.acs.org>.

## ■ AUTHOR INFORMATION

### Corresponding Author

[peter.mcbreen@chm.ulaval.ca](mailto:peter.mcbreen@chm.ulaval.ca); [hammer@phys.au.dk](mailto:hammer@phys.au.dk)

### Notes

The authors declare no competing financial interest.

## ■ ACKNOWLEDGMENTS

The work was supported by an NSERC Discovery Grant, CFI grants, and by the FQRNT Center in Green Chemistry and Catalysis (CCVC). This work was in part supported by the Lundbeck Foundation, the Danish Research Councils, and the Danish Center for Scientific Computing. V.D.-C. and G.G. acknowledge NSERC and FQRNT fellowships, respectively.

## ■ REFERENCES

- (1) (a) Stalcup, A. M. *Annu. Rev. Anal. Chem.* **2010**, *3*, 341. (b) Baddeley, C. J.; Richardson, N. V. In *Scanning Tunneling Microscopy in Surface Science, Nanoscience and Catalysis*; Bowker, M., Davies, P. R., Eds.; Wiley-VCH: Weinheim, 2010; pp 1–28.
- (2) Orito, Y.; Imai, S.; Niwa, S. *J. Chem. Soc. Jpn.* **1979**, *37*, 1118.
- (3) (a) Mallat, T.; Orglmeister, E.; Baiker, A. *Chem. Rev.* **2007**, *107*, 4863. (b) Bartok, M. *Curr. Org. Chem.* **2007**, *38*, 1533. (c) Blaser, H.-U.; Studer, M. *Acc. Chem. Res.* **2007**, *40*, 1348. (d) Murzin, D. Y.; Mäki-Arvela, P.; Salmi, T. *Catal. Rev.: Sci. Eng.* **2005**, *47*, 175. (e) Goubert, G.; McBreen, P. H. *ChemCatChem* **2013**, *5*, 683.
- (4) (a) Kyriakou, G.; Beaumont, S. K.; Lambert, R. M. *Langmuir* **2011**, *27*, 9687. (b) Taskinen, A.; Nieminen, V.; Hottokka, M.; Murzin, D. Y. *J. Phys. Chem. C* **2007**, *111*, 5128. (c) Bonalumi, N.; Bürgi, T.; Baiker, A. *J. Am. Chem. Soc.* **2003**, *125*, 13342. (d) Meemken, F.; Maeda, N.; Hungerbühler, K.; Baiker, A. *Angew. Chem., Int. Ed.* **2012**, *51*, 8212. (e) Baddeley, C.; Jones, T.; Trant, A.; Wilson, K. *Top. Catal.* **2011**, *54*, 1348–1356. (f) Gordon, A. D.; Zaera, F. *Angew. Chem. Int. Ed.* **2013**, *52*, 3453. (g) Lavoie, S.; Laliberté, M.-A.; Temprano, I.; McBreen, P. H. *J. Am. Chem. Soc.* **2006**, *128*, 7588–7593. (h) Bonello, J. M.; Williams, F. J.; Lambert, R. M. *J. Am. Chem. Soc.* **2003**, *125*, 2723–2729.
- (5) Demers-Carpentier, V.; Goubert, G.; Masini, F.; Lafleur-Lambert, R.; Dong, Y.; Lavoie, S.; Mahieu, G.; Boukouvalas, J.; Gao, H.; Rasmussen, A. M. H.; Ferrighi, L.; Pan, Y.; Hammer, B.; McBreen, P. H. *Science* **2011**, *334*, 776–780.
- (6) Orglmeister, E.; Mallat, T.; Baiker, A. *Adv. Synth. Catal.* **2005**, *347*, 78–86.
- (7) (a) Lavoie, S.; Laliberté, M.-A.; Mahieu, G.; Demers-Carpentier, V.; McBreen, P. H. *J. Am. Chem. Soc.* **2007**, *129*, 11668–11669. (b) Demers-Carpentier, V.; Laliberté, M.-A.; Lavoie, S.; Mahieu, G.; McBreen, P. H. *J. Phys. Chem. C* **2009**, *114*, 7291–7298. (c) Garvey,

M.; Bai, Y.; Boscoboinik, J. A.; Burkholder, L.; Sorensen, T. E.; Tysoe, W. T. *J. Phys. Chem. C* **2013**, *117*, 4505.

(8) Zhao, Y.; Truhlar, D. *Theor. Chem. Acc.* **2008**, *120*, 215–241.

(9) (a) Burkholder, L.; Garvey, M.; Weinert, M.; Tysoe, W. T. *J. Phys. Chem. C* **2011**, *115*, 8790–8797. (b) Boscoboinik, J. A.; Bai, Y.; Burkholder, L.; Tysoe, W. T. *J. Phys. Chem. C* **2011**, *115*, 16488–16494.

(10) (a) Vargas, A.; Bürgi, T.; Baiker, A. *J. Catal.* **2004**, *222*, 439–449. (b) Vargas, A.; Reimann, S.; Diezi, S.; Mallat, T.; Baiker, A. *J. Mol. Catal. A: Chem.* **2008**, *282*, 1–8. (c) Rasmussen, A. M. H.; Hammer, B. *J. Chem. Phys.* **2012**, *136*, 174706–174709. (d) Nieminen, V.; Taskinen, A.; Hottokka, M.; Murzin, D. Y. *J. Catal.* **2007**, *245*, 228–236.

(11) Knowles, R. R.; Jacobsen, E. N. *Proc. Natl. Acad. Sci. U.S.A.* **2010**, *107*, 20678–20685.

(12) Demers-Carpentier, V.; Laliberté, M.-A.; Pan, Y.; Mahieu, G.; Lavoie, S.; Goubert, G.; Hammer, B.; McBreen, P. H. *J. Phys. Chem. C* **2010**, *115*, 1355–1360.